J Mater Sci (2008) 43:2879–2888
DOI 10.1007/s10853-007-1968-0

An improved model for predicting fatigue S–N (stress–number of cycles to fail) behavior of glass fiber reinforced plastics

Michael Gary Wyzgoski · Glen E. Novak

Received: 30 January 2007 / Accepted: 25 June 2007 / Published online: 25 October 2007

Abstract In a previous study a model to predict the fatigue S–N behavior of glass fiber reinforced thermoplastics by using a fracture mechanics approach was presented. Using a single flaw size model, some degree of success was observed, particularly for a reinforced polyamide. The model was not successful in predicting the S–N behavior of a reinforced polyester. The earlier study also employed flexural fatigue rather than tensile fatigue data in the calculations because the calculated flaw sizes were more nearly constant as a function of stress level. Subsequently it was shown that the flexural fatigue stress calculations were in error for these types of short glass fiber reinforced plastics owing to the nonlinearity of their stress–strain behavior. In this report we reexamine the utility of the fracture mechanics approach to predict fatigue S–N behavior for both materials using an improved model. Whereas previously a single initial surface flaw was assumed, here we assume multiple flaws growing simultaneously across the sample thickness. The new model is applied to both flexural and tensile fatigue loading. Results demonstrate that this new approach provides accurate predictions of the S–N behavior for both materials under both loading conditions. This reflects the fact that the calculated initial flaw sizes are relatively independent of stress level. No additional adjustable parameters are required if one uses the initial breaking strength of the material as part of the model calculations.

M. G. Wyzgoski (✉) · G. E. Novak
Delphi Research Laboratories, Delphi Corporation,
51786 Shelby Parkway, Shelby Township, MI 48315, USA
e-mail: michael.g.wyzgoski@delphi.com

Introduction

This report is an extension of work done on the fatigue of glass fiber reinforced injection molded thermoplastics, which has been discussed at length by the authors [1–6]. Specifically, the earlier studies have demonstrated the value of using a fracture mechanics approach to characterize the fatigue fracture behavior of glass fiber reinforced thermoplastics.

For part design, one is generally more interested in fatigue S–N data under the conditions of use. This type of data is based upon measuring the number of cycles to fail, N, for a sample at various initial stress, S, levels. While the generation of such S–N data characterizes the materials fatigue resistance, it may require several months of testing time with multiple samples on relatively expensive servohydraulic testing equipment. Also the resultant data is highly dependent on the test conditions, e.g., load waveform, load range, temperature, frequency, etc. On the other hand, the generation of a fatigue crack growth rate curve requires a matter of hours with a single sample. Thus with this test method one can explore a variety of testing conditions much more rapidly.

Both methods have been utilized to characterize fatigue failure in metals [7, 8] and similarly both approaches have been described in the well known polymer fatigue text by Hertzberg and Manson [9]. As was pointed out earlier [1], strictly speaking, linear elastic fracture mechanics was not developed for inhomogeneous materials such as the glass fiber reinforced plastics described in this article. However, others have also found the theory to be useful for fatigue of composites [10].

It has been demonstrated in the literature how one could mathematically link the fatigue resistance measured by fatigue crack growth rates and S–N testing [9]. Therefore one can predict S–N behavior from the accelerated fatigue

crack growth rate data for a given material. Our first attempt to do this resulted in initial flaw size determinations, which, in some cases, were very dependent upon stress level [1]. Also, as a consequence of this stress dependence, the attempts to predict S–N behavior were not always successful. In the earlier report only flexural fatigue data were employed for S–N predictions since the flaw size results were better behaved.

In a separate study it was shown that the flexural fatigue data is in itself erroneous; because the linear elastic beam bending equations used to calculate flexural stress levels do not apply to these nonlinear materials [3]. An additional feature of flexural loading is that both tensile and compressive damage occur during loading. This factor can also influence and complicate the observed fatigue life, and argues once again for the use of the more straight forward tensile-tensile fatigue testing. In the present study the flaw sizes for both glass fiber reinforced PA (polyamide, nylon 66) and PBT (polybutylene terephthalate, polyester) are reexamined for both tensile and flexural loading using a more generalized fracture mechanics model. The intent is to obtain initial flaw sizes which are independent of stress level and to subsequently predict the fatigue S–N data from the accelerated fatigue crack propagation rate measurements without requiring additional adjustable parameters for the model.

Theory

While it has not been the intent of this predictive modeling effort to provide a detailed physical basis for interpreting the calculated flaw sizes in fiber reinforced plastics, the observed differences noted between tensile and flexural testing did suggest a new framework or approach. Specifically, in a three point bending test the region of maximum stress is very localized and tensile stress is imposed only on one surface of the specimen. In contrast, in a tensile test the stress is applied to a more extensive area of the specimen and is applied uniformly to all surfaces in the gage or narrow section of the specimen. It can be understood therefore why a model based upon the growth of a single flaw across the specimen thickness would likely be more successful for a bending type test. A cursory examination of tensile-tensile fatigue specimens reveals the general pattern that more flaw sites (stress whitened zones) occur at high stress, and fewer sites occur at lower stress levels. The new model proposed here is based upon the simple idea that multiple initial flaw sites either preexist or initiate and grow simultaneously until final failure. The linking together or coalescence of these multiple sites at final fracture implies that the final flaw size is therefore not a constant. Stated differently, the final flaw size can now be expected to be less than the specimen thickness as was assumed in the earlier study. The use of a variable final flaw size is the essential feature of the new approach proposed in this report.

The manner in which this idea modifies the calculation of flaw sizes and their use in predicting stress–lifetime curves first requires a review of the basic fracture mechanics theory. A more expanded discussion with reference to published texts [11–14] was provided earlier [1], but only the salient features are repeated here for readability. In fatigue crack propagation experiments, an intentional crack is introduced into the specimen. The fracture mechanics parameter, stress intensity factor, at the tip of a flaw or crack, is related to the more commonly measured imposed stress by the general expression:

$$K = Y\sigma\sqrt{a} \tag{1}$$

where:

K = stress intensity factor
Y = geometry factor
σ = stress
a = crack length

Y is a dimensionless factor, which can be obtained for specific geometries in handbooks [15]. It is known that the growth rate of a fatigue crack of length a, is well described by the stress intensity factor K, using the Paris Equation [9]:

$$\frac{da}{dN} = A\Delta K^m \tag{2}$$

where:

a = crack length
N = number of fatigue loading cycles
A = intercept of a log-log plot of da/dN versus ΔK
m = slope of log-log plot of da/dN versus ΔK

Combining this equation with the expression for K, after integration, allows us to relate the number of cycles to fail to the flaw sizes:

$$N_f = \frac{2}{(m-2)AY^m(\Delta\sigma)^m}\left(\frac{1}{a_0^{\frac{(m-2)}{2}}} - \frac{1}{a_f^{\frac{(m-2)}{2}}}\right) \tag{3}$$

Here N_f is the final or total number of cycles to fail and a_0 and a_f are the initial and final flaw sizes respectively. Previously we described how to use S–N and fatigue crack growth rate data to determine an initial flaw size for each material. The rearranged equation is

$$a_0 = \left(\frac{1}{\frac{N_f(m-2)AY^m\Delta\sigma}{2} + \frac{1}{a_f^{(m-2)/2}}}\right)^{2/(m-2)} \tag{4}$$

All parameters in the above equations except Y are experimentally determined in either the S–N test or the

crack propagation rate test. As reported previously a value of $Y = 1.17$ for a semicircular surface flaw was selected for all flaw size calculations [1, 15]. Again, the final flaw size, a_f, was previously assumed to be constant, equal to the sample thickness. The basic test of this model was then to assess the extent to which the calculated initial flaw sizes were independent of stress level, which would make it consistent with the fracture mechanics theory.

As mentioned earlier in the present study we now assume the final flaw size is dependent upon stress level. Unfortunately, without detailed microstructural characterization of the fatigue-tested specimens the mathematical relationship between the number of initial flaws (and thus the final flaw size) and stress level cannot be known. Therefore we have tested the variable final flaw size hypothesis by examining both a linear decrease in final flaw size with stress and also by assuming a more rapid exponential decrease. The latter, shown as Eq. (5) below, generally gave better "fits." For this function, the upper and lower bounds for a_f were fixed in the following way. For the case of maximum stress, defined by the monotonic or single cycle breaking stress, the value of a_f is set equal to a_0. In other words, the amount of fatigue crack growth is zero as the sample immediately fractures at this high stress level. At the other extreme, at low stress levels, a_f is set equal to the sample thickness, t. Although one might argue that this occurs at some slight positive stress, the analysis is simplified by setting a_f equal to t at zero stress. Figure 1 shows the assumed a_f variation schematically. Since the sample thickness and breaking stress are known parameters, this new approach requires no additional adjustable parameters compared to the earlier approach where a_f was treated as a constant. Using these assumptions, one obtains the following:

$$a_f = C_1 e^{-C_2 \sigma} \tag{5}$$

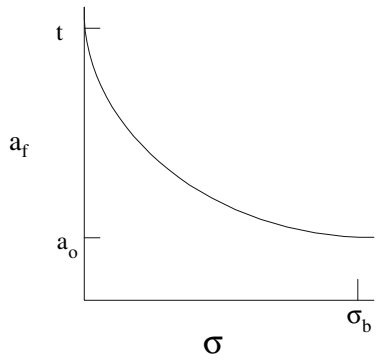

Fig. 1 Proposed variation of final flaw size with stress level. Symbols defined in text

where

$$C_1 = t \tag{6}$$

and

$$C_2 = \frac{[\ln(t) - \ln(a_0)]}{[(\sigma_B)]} \tag{7}$$

where again:

a_0 = initial flaw size
a_f = final flaw size
t = thickness
σ_B = breaking stress

This expression for a_f is inserted into Eq. (4) for a_0. An iterative solution is now required since a_f is a function of a_0. However, as noted above, the values for C_1 and C_2 are specified in terms of the specimen thickness and material breaking stress making the calculations straightforward. Finally, once the full range of values for a_0 is obtained, an average value can be determined, and this average value can be used in Eq. (3) to calculate an S–N curve for comparison with the original S–N data. While the latter comparison is ultimately the best way to assess the validity of the fracture mechanics approach, the accuracy of the prediction reflects how well the initial flaw size is a constant value, independent of stress.

Experimental

The materials, description of specimen preparation methods, and most fatigue data were taken from the earlier study [1]. The two materials reexamined in this study included the 33 wt.% glass filled nylon 66 polyamide, PA, DuPont's Zytel 70G33L; and the 30 wt.% glass filled polybutylene terephthalate, PBT, General Electric's Valox 420. Samples for fatigue S–N tests and crack growth rate measurements had been cut from a specially designed ribbed plaque. In addition, ASTM Type I injection molded tensile bars of the filled PBT were also fatigue tested for this study. For the latter, S–N testing was performed at 5 Hz in tension-tension loading at an R-ratio of 0.1.

Results

Nomenclature

The terms flow and Xflow are defined as follows. For flow specimens the axis of imposed stress is parallel to the melt flow direction, which is also the predominant fiber orientation direction. Thus for flow specimens the fatigue crack growth direction is transverse to the aligned fibers and

these specimens should exhibit maximum fatigue resistance. Xflow specimens are cut orthogonal to the flow specimens.

Paris Equation constants

Table 1 lists the A and m values for the Paris Equation (Eq. (2), this report) fitting of the fatigue crack propagation rate data for PA and PBT for the crossflow and flow directions [1]. In addition, the results for PBT were reinterpreted after recognizing that a slope change or discontinuity occurred for all samples at a particular region of the da/dN–ΔK plot. The slight shift, suggesting a deceleration, can be seen in the previously reported data [1]. A review of all PBT data showed this feature to be very reproducible, occurring at the same region of ΔK, regardless of frequency. Although the slope change occurs in the midpoint of the ΔK range, this latter part of the da/dN plot represented only the last 20 min of an approximately 8-h test. Similar shifts were not observed in da/dN plots for other materials. Also, the linear fit of the entire da/dN–ΔK data for PBT had resulted in a lower slope and a lower correlation coefficient [1]. A possible explanation is crack tip blunting with rapid tearing in the more ductile PBT matrix material at the end of the test, but at present we can offer no evidence to corroborate this. Because of the anomaly, and poor fit to the Paris Equation constants, the latter were recalculated for the PBT without this high ΔK data. The result is shown in Fig. 2, and the recalculated m and A values are also listed in Table 1 as Low ΔK values. For the latter, the slope, m, is significantly increased, and the intercept is decreased.

PBT flaw size determinations and S–N predictions

We begin by recalculating flaw sizes for the glass fiber reinforced PBT material using the flexural fatigue S–N data for the case of the crossflow orientation. This material provided the worst predictive results previously. Figure 3 shows the dependence of initial flaw size on stress level for both the previous constant final flaw size and the present

Table 1 Fatigue crack growth parameters

Material	Orientation	A (m/cycle)	m
PA	Flow	2.6 E-13	9.32
	Xflow	4.9 E-12	9.32
PBT	Flow	7.92 E-12	7.41
	Xflow	1.53 E-10	7.41
PBT-low ΔK	Flow	9.02 E-14	10.6
	Xflow	6.21 E-12	10.6

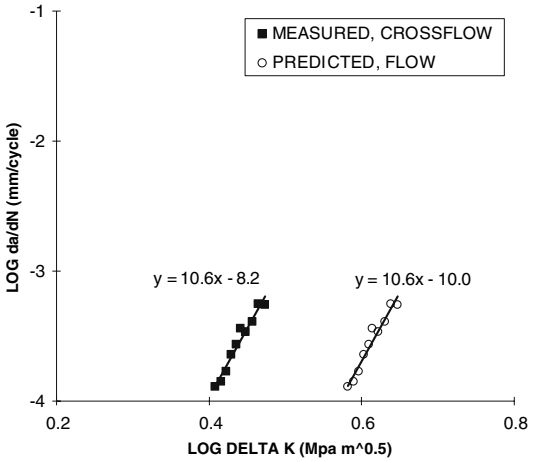

Fig. 2 Refit of Paris Equation to lower ΔK data in da/dN plot for PBT

variable final flaw size models for the crossflow orientation. The initial flaw size is much less dependent upon stress level using the variable final flaw size model. Also shown in Fig. 3 are the results for the PBT in this orientation using the redefined Paris Equation constants at low ΔK. While the latter provides an increase in the calculated initial flaw sizes, it also results in values that are less dependent upon stress level.

To validate the fracture mechanics approach the average calculated flaw sizes are used with Eq. (3) to determine a predicted S–N curve. In earlier work [1], the average was sometimes based upon only the lower stress levels, particularly when the initial flaw size appeared more constant only at these stress levels. For this report, all of the predicted S–N curves employ a simple numerical average of all the initial flaw sizes over the entire stress range. Table 2 is a summary of the calculated average initial flaw sizes for both materials for the different loading and different flow directions.

In Fig. 4a the S–N predictions are shown for the constant final flaw size model with and without the advantage of using the recalculated Paris Equation constants from the

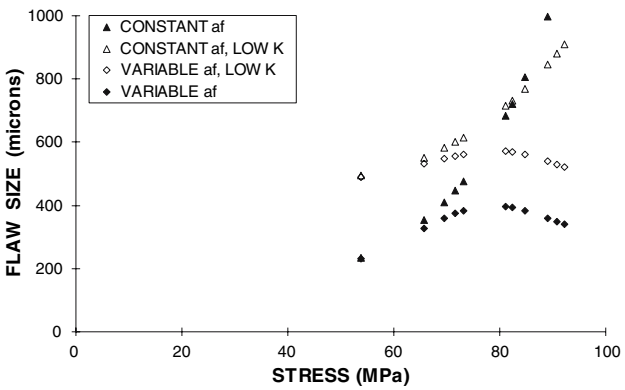

Fig. 3 Initial flaw sizes for PBT using crossflow flexural S–N data

Table 2 Calculated flaw sizes

Material	Stress	Orientation	Flaw size			
			Constant a_f		Variable a_f	
			a_0	a_f	a_0	a_f
PA	Tensile	Flow	583	2,500	552	598–1,462
	Tensile	Xflow	823	2,500	734	786–1,450
	Flex	Flow	201	2,500	198	266–1,080
	Flex	Xflow	424	2,500	400	423–1,262
PBT	Tensile	Flow	1,500	2,400	1,041	1,071–1,686
	Tensile	Xflow	1,443	2,400	936	972–1,564
	Flex	Flow	419	2,400	260	277–951
	Flex	Xflow	670	2,400	354	370–942
Low ΔK	Tensile	Flow	1,730	2,400	1,414	1,440–1,859
	Tensile	Xflow	1,805	2,400	1,350	1,383–1,743
	Flex	Flow	473	2,400	398	415–994
	Flex	Xflow	700	2,400	544	563–1,162
Tensile bars						
No holes	Tensile	Flow			1,555	1,646–2,340
Holes	Tensile	Flow			1,871	2,049–3,001

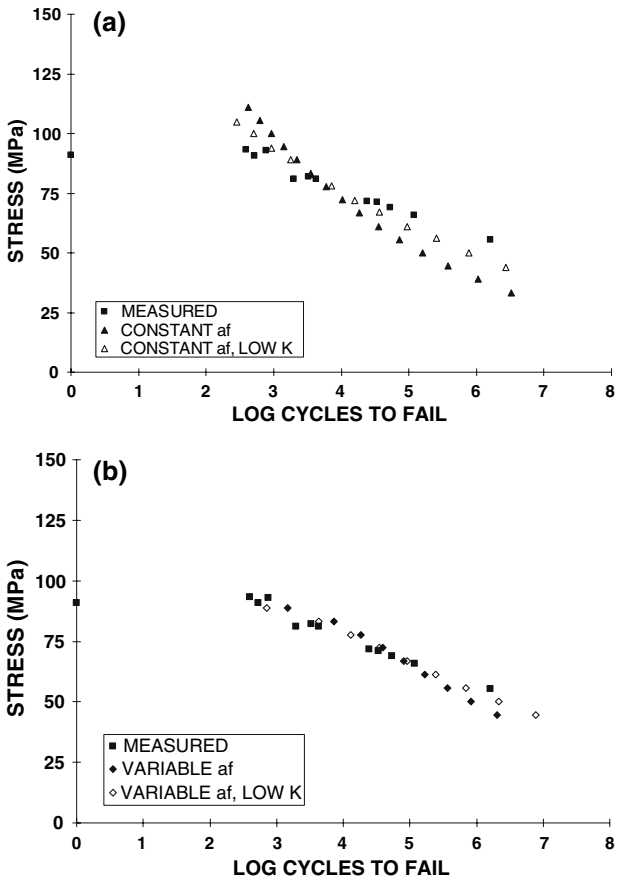

Fig. 4 (**a**) Predicted versus measured crossflow flexural S–N for PBT using constant af. (**b**) Predicted versus measured crossflow flexural S–N for PBT using variable a_f

low ΔK da/dN data. Some improvement is noted for the former but the results are still unsatisfactory. Figure 4b demonstrates that the variable final flaw size model provides a much better fit to the measurements. An apparent anomaly in Fig. 4 and in some subsequent figures is that the single cycle breaking stress is equal to or less than some of the low cycle fatigue data points. Possible explanations for this are (1) the single cycle test is conducted at a strain rate approximately an order of magnitude lower than the fatigue test, and (2) the fatigue data points are for only a few hundred cycles and exhibit significant scatter. Further testing is required to provide an explanation.

For the case of the flow direction, it should be recalled that the fatigue crack growth rate data must itself be predicted as demonstrated in Fig. 2. The predicted da/dN data is based upon the strain energy release rate calculation previously reported [6] which requires only modulus and Poisson's ratio data to shift the crossflow da/dN data. The variable final flaw size approach again leads to a value of initial flaw size which is relatively independent of the stress level. Figure 5 shows the corresponding S–N predictions for the various cases. As with the case for the crossflow-oriented specimens, it is again seen, in Fig. 5a, that the use of the recalculated Paris Equation low ΔK da/dN data improves the predictions somewhat. However, as shown in Fig. 5b, the best or optimum fit once more is obtained using both the low ΔK constants and the variable final flaw size approach to make the S–N prediction.

For the tensile S–N data for PBT the recalculated initial flaw sizes are shown in Fig. 6 for the case of the crossflow

orientation. As with the flexural data, the variable flaw size approach leads to relatively constant values for the initial flaw sizes versus stress level. The magnitude of the initial flaw size is increased significantly and in many cases seems unrealistically high, approaching the thickness of the samples. However the variable final flaw size approach has the desired effect of removing the stress dependency of the initial flaw size, thus making it more realistic to represent the initial flaw size with a single average value. As with the flexural S–N data, the predictions of tensile S–N results for PBT in the crossflow orientation are relatively poor for the constant final flaw size approach (Fig. 7a), and are excellent for the variable final flaw size approach (Fig. 7b). In fact, for the latter, the primary difference in the use of either the low ΔK da/dN or the entire da/dN dataset to determine Paris Equation constants, and subsequent flaw sizes, is the long-term S–N lifetime predictions (1 million cycles). For these longer lifetimes, experimental data are not available. The use of both the new approach and low ΔK data gives the best result.

For the flow direction tensile S–N results, similar conclusions are drawn from the flaw size calculations. Figure 8a and b show the S–N predictions. Once again the variable final flaw size approach gives better predictions of the measured S–N. Whether the long lifetime predictions are overly conservative or not depends on the validity of the single measured data point at about 1 million cycles. This is further discussed in a later section.

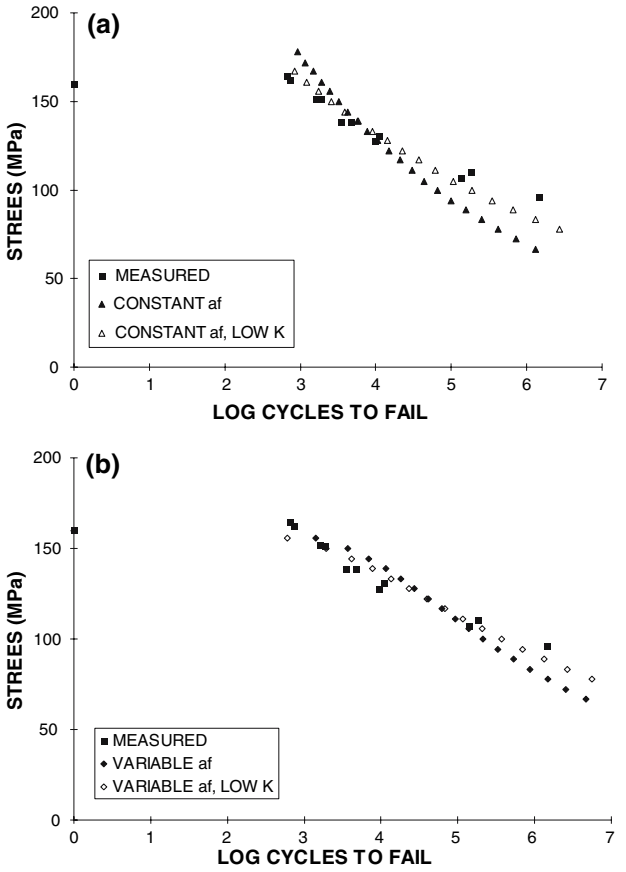

Fig. 5 (**a**) Predicted versus measured flow flexural S–N data for PBT using constant a_f. (**b**) Predicted versus measured flow flexural S–N for PBT using variable a_f

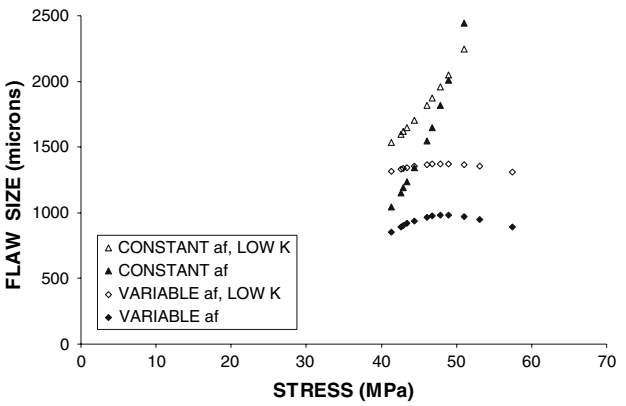

Fig. 6 Initial flaw sizes for PBT based upon crossflow tensile S–N data

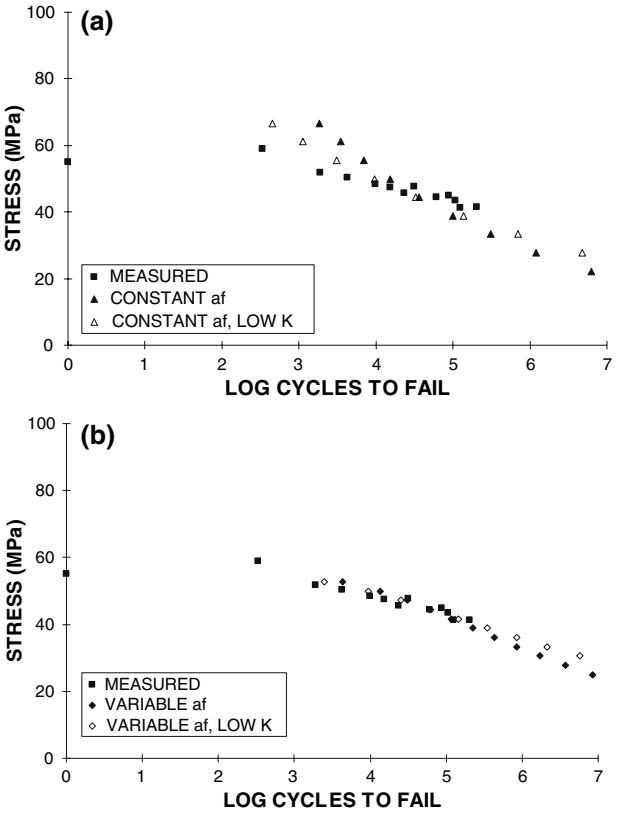

Fig. 7 (**a**) Predicted versus measured crossflow tensile S–N for PBT using constant a_f. (**b**) Predicted versus measured crossflow tensile S–N for PBT using variable a_f

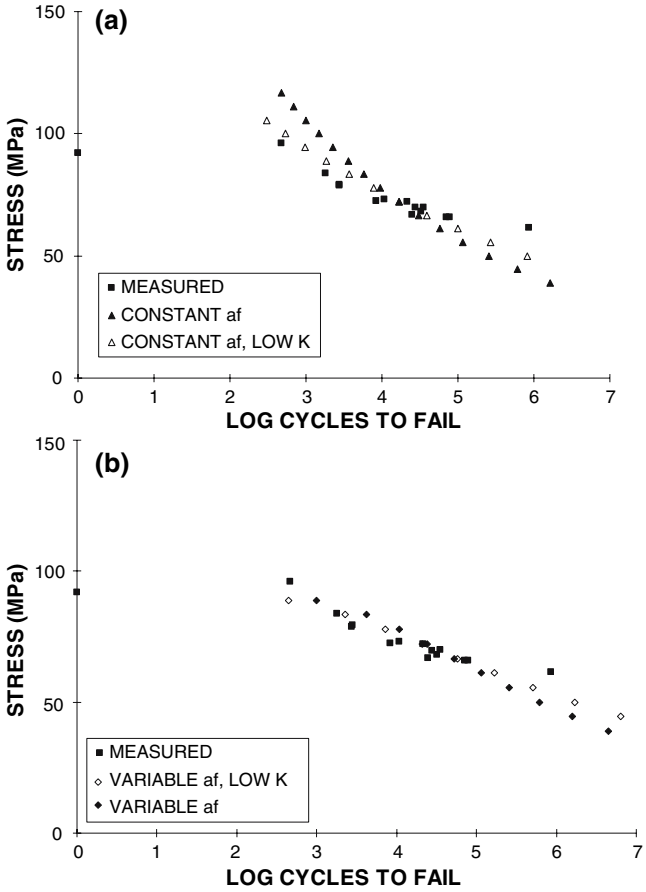

Fig. 8 (**a**) Predicted versus measured flow tensile S–N for PBT using constant a_f. (**b**) Predicted versus measured flow tensile S–N for PBT using variable a_f

PA flaw size determinations and S–N predictions

Previously, it was demonstrated that the constant final flaw size approach gave very good results with PA for the case of the flexural S–N [1]. Excellent results were also obtained using the new variable final flaw size approach for the PA material. For the sake of brevity, these data are not replotted here.

In the case of the tensile S–N behavior for PA, the use of the variable final flaw size approach is seen in Fig. 9 to have the desired effect, namely, the initial flaw size is less stress dependent for both crossflow and flow orientations, slightly more so for the former. The change in stress dependence and subsequent average flaw size, produce some improvement in the predicted S–N behavior as shown in Figs. 10 and 11. While the results for the crossflow case are very good, the flow direction predictions, although satisfactory, are not as accurate. Also, when comparing the previously reported flexural S–N predictions for PA in the flow direction with the tensile S–N predictions, the former are much more accurate. This is believed to be related to the localization of stress in the flexural tests as noted earlier in the Theory section.

Localized versus uniform tensile stress in the S–N test

An additional experiment was performed to shed more light on the role of a uniform versus a localized stress on the S–N predictions. Injection molded PBT tensile bars

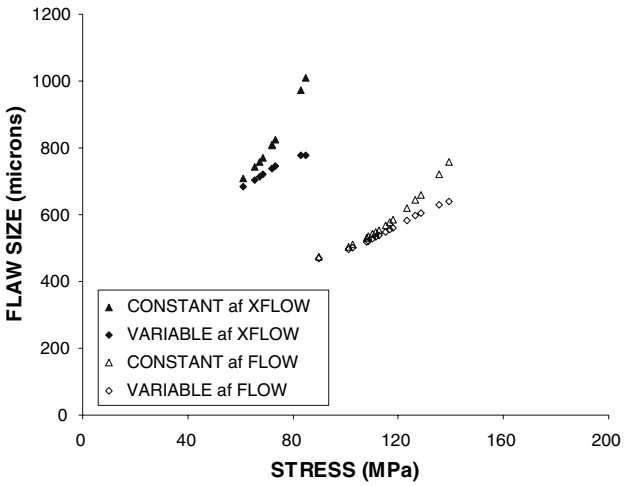

Fig. 9 Initial flaw sizes for PA based upon both crossflow and flow tensile S–N data

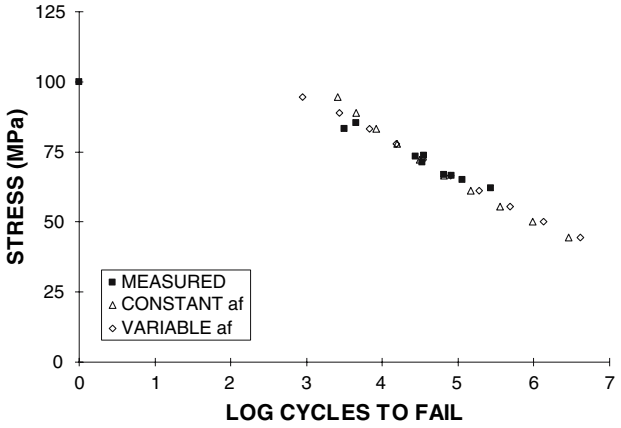

Fig. 10 Predicted versus measured crossflow tensile S–N for PA

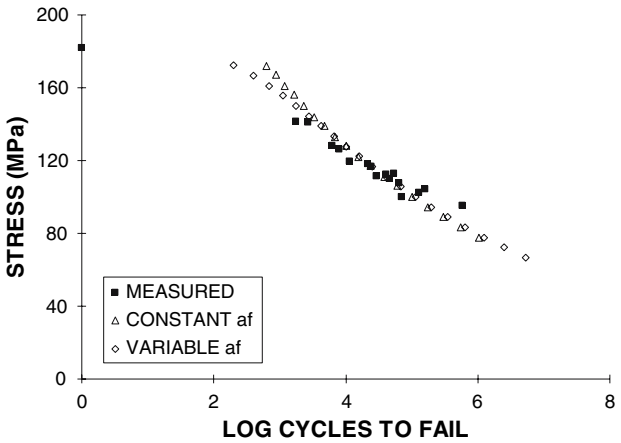

Fig. 11 Predicted versus measured flow tensile S–N for PA

were used to generate an S–N curve and also the same bars were fatigued after creating a localized stress concentration with a drilled hole. The hole diameter was 3.2 mm, which is also equal to the thickness of the tensile bars. The relative stress concentration of the hole was determined by using the breaking stress ratio between samples with and without holes. This gives a stress concentration factor of 1.27 for the hole based upon the net cross sectional area. Of interest to the present discussion are the S–N predictions for the tensile bars with and without holes. For samples with holes, the thickness used in calculating flaw sizes is the residual width, since cracks grow from the hole edge outward. This is shown in Fig. 12 and is are based upon using the same flow direction crack propagation rate predictions as used previously for the samples cut from plaques. For the tensile bars without holes, the predicted S–N generally had captured the measured results (Fig. 8b). However, a closer examination indicates that results are over predicted at high stress levels and under predicted at low stress levels. Note that the shape of the predicted curve in Fig. 12 matches the

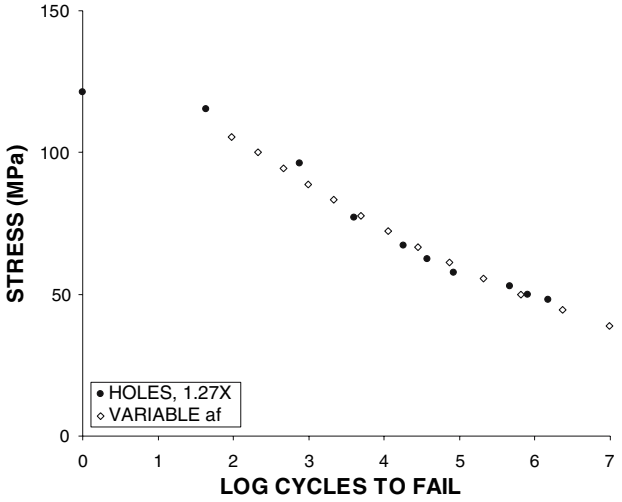

Fig. 12 Predicted versus measured S–N for PBT tensile bars with holes after correcting for stress concentration factor of hole

stress corrected S–N data very well for the samples with holes. This suggests that under tensile loading the model provides more accurate predictions when the stress is more localized, similar to the case of flexural loading.

Summary plots for flow direction

It is of interest to compare the different measured fatigue S–N data sets with the prediction of the proposed model for the plaques in the flow direction. This is shown in Fig. 13 for the PBT and in Fig. 14 for the PA. In each case the flexural fatigue data was first corrected for the material's plasticity-like behavior as described above. At long lifetimes the PBT prediction is conservative. This appears to be

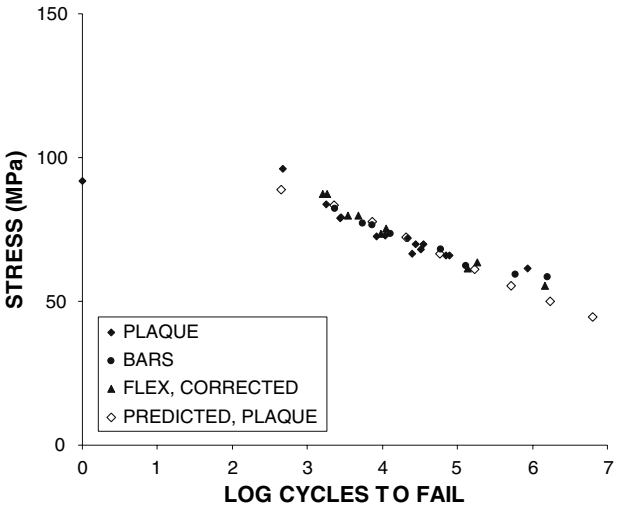

Fig. 13 Summary plot of PBT flow S–N measurements versus prediction

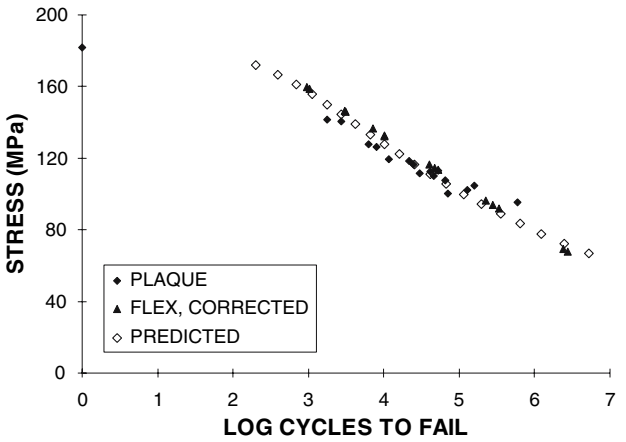

Fig. 14 Summary plot of PA flow S–N measurements versus prediction

true for the PA also, although less data are available to make this conclusive. This is considered a good feature since it provides a factor of safety in the predictions. For both materials the predictions in Figs. 13 and 14 based upon the plaque tensile fatigue represent the various data sets well.

Discussion

Constant versus variable final flaw size

The impetus for this study was both the poor S–N predictions using the constant final flaw size fracture mechanics approach for the PBT material, and the similar poor fit when this model was applied to tensile S–N data. The latter shortcoming is exacerbated by the realization that the common practice for calculating flexural fatigue stress for fatigue or flexural strength is in error for these glass-reinforced thermoplastics [3]. Thus, tensile fatigue is to be preferred. The present study indicates that the variable final flaw size approach has advantages in improving the S–N predictions. While there was some improvement for the PBT material by recognizing the need to recalculate the Paris Equation parameters from the fatigue crack growth rate data, the best fit was always obtained with the combined use of these new parameters with the variable final flaw size model. The benefits of the new model for the PA material under flexural fatigue were minor, because excellent results were already shown with the earlier model [1], however, the new model is preferred because it can be used for all loading conditions and materials.

Magnitude of the flaw sizes

As in the past, we do not attempt to put a physical interpretation on the measured initial or final flaw sizes or worry about the relative amounts of crack growth for each material and type of loading. The magnitude of the flaw sizes will depend on many factors including the choice of the geometry factor, Y, the type of assumed initial flaw, and the assumptions regarding the final flaw size limits. Also the magnitude of the final flaw sizes and subsequent S–N predictions are very sensitive to the crack growth exponent, m. While this provides a valid argument against utilizing the approach presented here, our view is that the benefits outweigh the limitations. Our purpose for developing a model is to reproduce the S–N data with a reasonable accuracy using the single set of fatigue crack growth rate measurements and obtain the necessary fitting constants, in this case, average initial flaw sizes. With this information it is then possible to make predictions for other load ratios, frequencies, temperatures, effects of humidity, etc. Some of these predictions will require a remeasurement of the basic crack growth rate curve under the new conditions, but crack growth rate measurements are a greatly accelerated test compared to generating an entire S–N curve. Also, without any additional experimental measurements the effects of fiber orientation can be estimated by either averaging the initial flaw sizes for flow and xflow or using the smaller value to make a conservative prediction. Of course, with the added value of the strain energy release rate model [6] for calculating fatigue crack growth rate curves for other fiber loading levels or even fiber types, S–N predictions or estimates can be made for many other material options.

Recommended practice

It is difficult to draw general conclusions based upon the extensive analyses of only two glass reinforced materials at one glass content. However it is also important to provide the reader with our view on how any new material should be approached to provide a database and predictive methodology for fatigue design of injection molded parts. Based upon the results of this study, particularly Figs. 13 and 14, the following is recommended. Injection mold ISO Standard plaques [16] using very slow fill speeds and at a thickness not to exceed 2 mm. This will provide a maximum anisotropy representative of many typical injection molded components, which may be 3 mm or thicker. Mill cut ISO Type 1BA specimens in both flow and crossflow directions per the template provided in the ISO Standard. Obtain tensile property data for both orientations including Poisson's ratio following the usual ASTM or ISO Standards. Perform tensile-tensile fatigue at an R-ratio of 0.1 and 5 Hz. Obtain fatigue crack propagation rate data for compact tension specimens cut from the ISO plaque for the crossflow orientation at $R = 0.1$ and 0.5 Hz. The lower

frequency for crack propagation rate measurements is owing to the greater sensitivity to hysteretic heating at the crack tip in this geometry. While there is no standard for the latter we have described our procedure earlier [1, 5, 6]. Predict the flow direction fatigue crack growth rate data using the strain energy release rate model calculations after measuring the flow direction modulus and Poisson's ratio. Use the analysis presented here to combine the crack growth data with the S–N data for determination of flaw sizes for both the flow and crossflow orientations. Calculate S–N data for comparison with measured results to confirm the validity of the calculated flaw sizes. Utilize the flaw sizes as a material constant for making S–N predictions for other material compositions or fiber orientations as discussed previously in this section.

Conclusions

1. Fatigue lifetime predictions for both materials in many cases are indistinguishable from the actual measured data. By contrast, the lifetime predictions of the earlier model could deviate by more than an order of magnitude from the measured data.
2. The calculated initial flaw sizes are generally more independent of stress level as required by fracture mechanic theory.
3. No additional adjustable parameters are required if one uses the initial breaking strength of the material as part of the new model calculations.

Acknowledgements The authors wish to thank Professor J. Gordon Williams of Imperial College for most helpful discussions concerning the application of fracture mechanics principles to reinforced thermoplastics.

References

1. Wyzgoski MG, Novak GE (2005) J Mater Sci 40:295, DOI: 10.1007/s10853-005-6082-6
2. Wyzgoski MG, Krohn JA, Novak GE (2004) Polym Composites 25(5):489
3. Wyzgoski MG, Krohn JA, Novak GE (2004) Polym Composites 25(6):569
4. Martin DC, Novak GE, Wyzgoski MG (1989) J Appl Polym Sci 37:3029
5. Wyzgoski MG, Novak GE (1995) Polymer Composites 16(1):38
6. Wyzgoski MG, Novak GE (1991) J Mater Sci 26:6314, DOI: 10.1007/BF02387810
7. Dowling NE (1993) Mechanical behavior of materials. Prentice Hall
8. SAE Fatigue Design Handbook (1988) AE-10, 2nd edn
9. Hertzberg RW, Manson JA (1984) Fatigue of engineering plastics. Academic Press, p 74
10. Reifsnider KL (ed) (1991) Fatigue of composite materials. Elsevier
11. Kinloch AJ, Young RJ (1983) Fracture behavior of polymers. Applied Science
12. Williams JG (1984) Fracture mechanics of polymers. Ellis Norwood Lmt
13. Friedrich K (ed) (1989) Composite materials series, 6: application of fracture mechanics to composite materials. Elsevier
14. Moore DR, Pavan A, Williams JG (eds) (2001) ESIS Publication 28: fracture mechanics testing for polymers, adhesives and composites. Elsevier
15. Murakami Y (ed) (1987) Stress intensity factors handbook. Pergamon Press
16. International Standards Organization Standard, ISO 294-5 (2001) Preparation of Standard Specimens for Investigating Anisotropy